SCIENTIFIC REPORTS

OPEN

SUBJECT AREAS:
THEORY AND COMPUTATION
METAL-ORGANIC FRAMEWORKS

Received
26 November 2013

Accepted
28 January 2014

Published
14 February 2014

Correspondence and requests for materials should be addressed to Q.S. (sunqiang@pku.edu.cn)

The superior catalytic CO oxidation capacity of a Cr-phthalocyanine porous sheet

Yawei Li[1] & Qiang Sun[1,2]

[1]Department of Materials Science and Engineering, College of Engineering, Peking University, Beijing 100871, China, [2]Center for Applied Physics and Technology, Peking University, Beijing 100871, China.

Two-dimensional organometallic sheets containing regularly and separately distributed transition atoms (TMs) have received tremendous attentions due to their flexibility in synthesis, well-defined geometry and the promising applications in hydrogen storage, electronic circuits, quantum Hall effect, and spintronics. Here for the first time we present a study on the superior catalytic CO oxidation capacity of a Cr-phthalocyanine porous sheet proceeding first via Langmuir-Hinshelwood (LH) mechanism and then via Eley-Rideal (ER) mechanism. Compared to the noble metal based catalysts or graphene supported catalysts, our studied system has following unique features: without poisoning effect and clustering problem, having comparable reaction energy barrier for low-temperature oxidation, and low cost for large-scale catalytic CO oxidation in industry.

The catalytic oxidation of carbon monoxide (CO) has attracted extensive attentions for several decades due to its crucial role in exhaust treatment of the post-combustion process for automobiles[1] as well as in alleviating the poisoning effect on methanol fuel cell electrocatalysts[2], it is also a prototype catalytic reaction in surface chemistry because of its stoichiometric simplicity as well as industrial significance, which plays an essential role in evaluating catalyst activity, selectivity and durability. Following the pioneering work on Pt wires of Langmuir[3], many noble metals such as Pt[4,5], Rh[6,7], Pd[7] and Au nanoparticles[8–10] are studied for catalyzing CO oxidation. However, these catalysts are generally costly, and platinum based catalysts usually encounter CO poisoning problems, impeding durable operation. To overcome this problem, novel low dimensional nanocatalysts including metal embedded graphene[11–16] as well as metal embedded carbon nanotubes (CNTs)[16] have been suggested for enhancing the catalytic activity of CO oxidation with considerably low energy barriers[12–16]. However, it is technically difficult to controllably generate such defects in these materials. In fact, previous calculations revealed that the formation energy of a single vacancy (SV) or a double vacancy (DV) in graphene can be as high as about 7.5 ~ 8.0 eV[17]. So it is highly desirable to develop novel porous organometallic materials intrinsically containing *exposed* metal cations for large-scale catalytic CO oxidation in industry.

The recent success in embedding Fe atoms into a 2D polymeric phthalocyanine (Pc) sheet[18] inspired us to employ metal-phthalocyanine-based sheets as the candidates of low-temperature CO oxidation catalysts. Indeed, various experimental[19–24] and theoretical[25–27] efforts have been devoted to unveil the observed catalytic activities of molecular transition metal phthalocyanine compounds towards oxygen reduction reaction and CO_2 reduction reaction. The 2D Pc sheets, as illustrated in Figure 1, are superior to defected graphene/CNTs based systems due to the following reasons: First, the synthesis procedure of 2D FePc framework is flexible for other TM elements, indicating that other 2D TMPc sheets are able to be synthesized in the future. Second, the structural motif of 2D FePc framework highly resembles biological metalloporphyrin systems such as hemoglobin, where the kernel of hemoglobin possesses strong binding affinity to CO and O_2[28]. Therefore, it seems plausible to assume that certain kinds of 2D TMPc sheets can also reversibly bind CO and O_2 ligands, which acts as an indispensible prerequisite in the whole catalytic CO oxidation process. Third, the electronic states of TM atoms can be effectively tuned by the Pc square planar ligand field and by varying the metal atom at the Pc center[29], enabling us to systematically investigate the catalytic behavior of various 2D TMPc sheets. Although the basic magnetic properties, intrinsic magnetic couplings and gas storage properties of 2D TMPc frameworks have been thoroughly investigated[30–35], the possibility of such systems for catalyzing CO oxidation and their corresponding reaction mechanisms have not been well addressed yet.

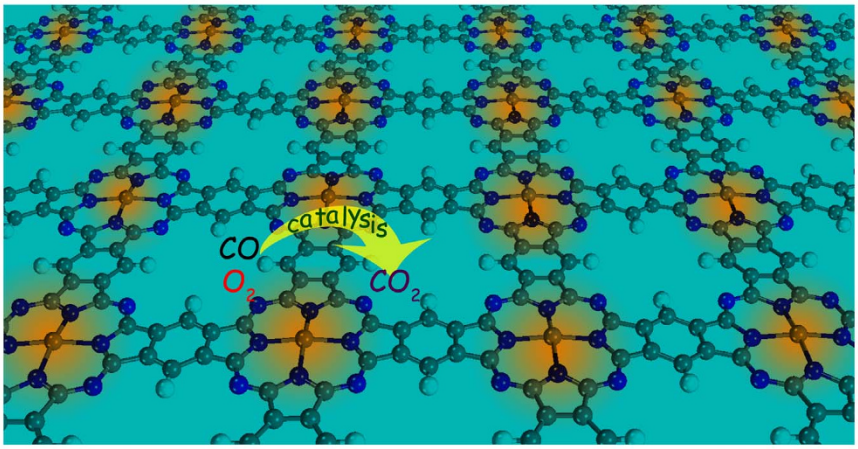

Figure 1 | Schematic illustration of 2D TMPc sheet and its catalytic behavior toward CO oxidation. The highlighted areas denote the most catalytically active sites.

In this work, we performed first-principles calculations to systematically investigate the catalytic feature for CO oxidation of the 2D TMPc sheets. We chose TM atoms in the 3d series ranging from Cr to Cu. Among them, the 2D CrPc sheet is identified as a potential candidate for low-temperature CO oxidation, exhibiting the highest catalytic activity without the CO poisoning effect. Previous density functional calculations reveal that TiO_2(110) or MgO(100) supported model Au nanoparticle catalysts can accelerate CO low-temperature oxidation with energy barriers of 0.35 ~ 0.75 eV[9,36,37]. For free-standing Au nanoparticles the energy barriers are even larger (0.46 ~ 1.03 eV)[38]. Using the same level of theory, we found that 2D CrPc can catalyze CO oxidation with an energy barrier of 0.55 eV, comparable with those of supported Au nanoparticles. The different extents of the hybridizations between CO/O_2 frontier orbitals and the TM d states are predominantly responsible for the observed trends in the adsorption energies of both CO and O_2 on different 2D TMPc sheets. The reaction of CO and O_2 on 2D CrPc sheets proceeds via two steps, namely the LH mechanism followed by the ER mechanism. We further provided detailed analyses on the electronic structure of the 2D CrPc system in the LH reaction processes to elucidate the superb catalytic activity exhibited in the 2D CrPc sheet.

Results

Searching for the candidate. Before examining the CO oxidation reaction paths on 2D TMPc sheets, we first studied CO and O_2 adsorption on these frameworks. The adsorption energy of an adsorbate is defined as $E_{ad} = E_{TMPc + mol} - E_{TMPc} - E_{mol}$, where $E_{TMPc + mol}$, E_{TMPc} and E_{mol} are the total energies of the 2D TMPc with the adsorbed molecule, the isolated 2D TMPc and the isolated gas molecule, respectively. By this definition, negative (positive) values of E_{ad} represent exothermic (endothermic) adsorption processes. The variation of $E_{ad}(CO)$ and $E_{ad}(O_2)$ in different 2D TMPc framework is illustrated in Figure 2. Both $E_{ad}(CO)$ and $E_{ad}(O_2)$ undergo a giant reduction in their absolute values when changing the central TM atom from Fe to Co. However, CO adsorption is appreciably enhanced while the binding to O_2 adsorption is only weakly attenuated when the TM atom is changed from Cr to Fe, resulting favored bindings to CO in MnPc and FePc 2D frameworks.

From the above analyses we can see that among all of the studied systems, only the 2D CrPc, MnPc and FePc systems are likely to become the candidates of low-temperature CO oxidation catalysts, arising from the strong interaction between such 2D porous sheets and CO as well as O_2. Next we focus on another important factor which affects the durability of the CO oxidation catalysts, namely the CO poisoning effect. Because $E_{ad}(CO)$ is larger than $E_{ad}(O_2)$, the MnPc and FePc sheets will be dominantly covered by CO if the 1 : 1 CO/O_2 mixture is injected with a constant gas flow rate. In this condition, the MnPc and FePc sheets adsorbed with CO will not suffer from the poisoning effect only when it is exothermic for those CO-covered 2D frameworks to bind O_2 molecules and form coadsorption states. To this end, we define $E_{coad} = E_{TMPc+CO+O_2} - E_{TMPc+CO} - E_{O_2}$, where $E_{TMPc+CO+O_2}$, $E_{TMPc + CO}$ and E_{O_2} denote the total energies of the CO/O_2coadsorbed on 2D TMPc, CO adsorbed 2D TMPc and free-standing O_2 molecule, respectively. The negative values of E_{coad} would suggest the feasibility of removing CO from the 2D TMPc sheets. Our calculation results indicate that the FePc sheet is unable to form such a stable coadsorption state. Furthermore, although the coadsorption state can exist in the MnPc sheet, the E_{coad} value of the MnPc sheet is 0.92 eV. Therefore, both of the two sheets are susceptible to CO poisoning in catalyzing the CO oxidation reaction, indicating that they cannot be employed as CO oxidation catalysts. In contrast to these two sheets, the catalytic active sites in a the CrPc sheet are much more stable towards irreversible CO binding with a negative E_{coad} of −0.16 eV, suggesting that only the CrPc sheet can be applied to catalytic oxidation of CO with negligible CO poisoning effect.

The distinct adsorption behaviors of CO and O_2 can be rationalized through the analysis of the spin-polarized orbital of 2D TMPc sheets at the Γ point. The selected orbital energy levels of CrPc, FePc with their corresponding electron density distributions are illustrated in Figure 3a and 3b. Generally, a chemical reaction cannot change the overall spin of the system due to the Wigner-Witmer rules

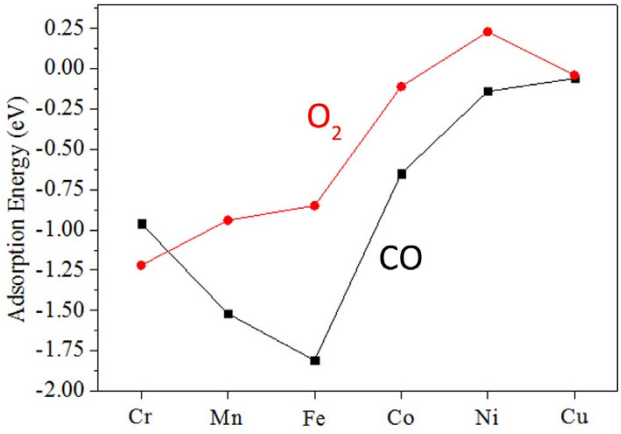

Figure 2 | Adsorption energies (E_{ad}) of CO and O_2 adsorbed on 2D TMPc.

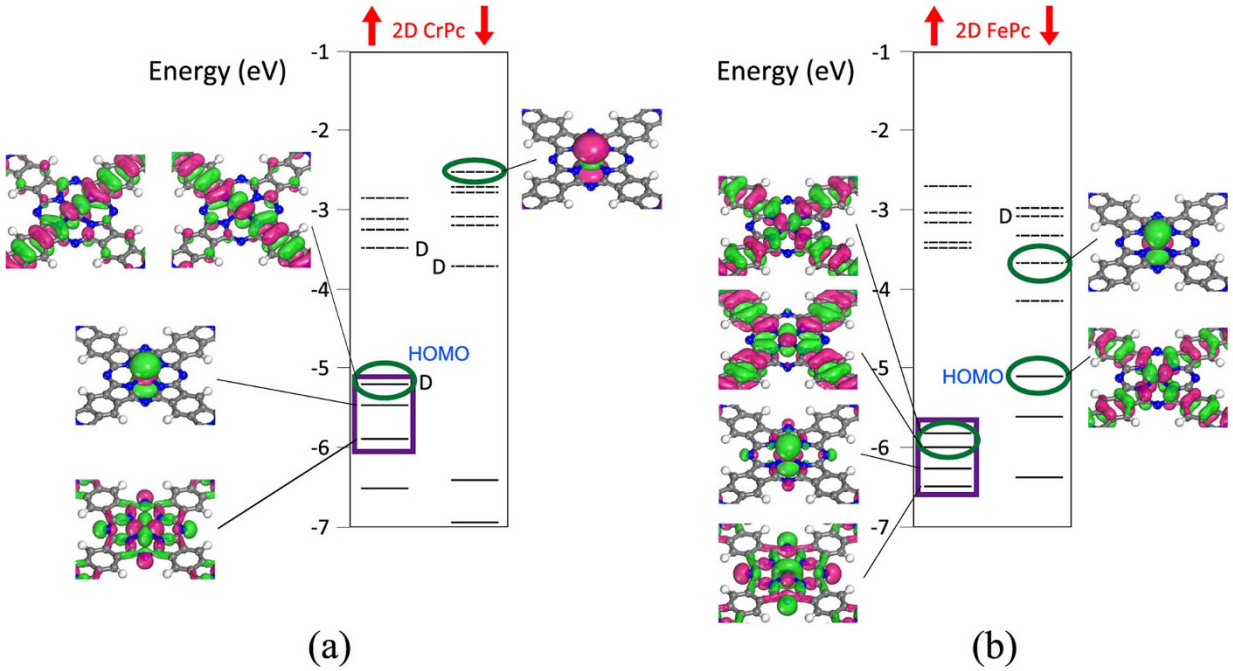

Figure 3 | Electron energy levels and orbital charge density isosurfaces (isovalue 0.02 coulomb/m^3) in 2D CrPc and 2D FePc sheets. The arrows denote the spin-up and spin-down. The solid lines correspond to the filled levels and the dotted lines to the unfilled levels. The doubly degenerate levels are marked with upper-case letter D. The lines in the rectangles denote levels interacting with O_2 2π* levels and those in the ovals denote levels interacting with CO 5σ and 2π* levels.

of spin conservation[39–41]. Nonetheless, for systems such as TMPc sheets, the central transition metal atoms exhibit a modest extent of spin-orbit effects, enabling them to undergo spin-forbidden transitions to achieve a so-called spin inversion. Although the spin-orbit interaction is generally regarded to play a key role in mediating the spin inversion in reactions containing TM elements, for the 3d transition metals, this interaction alone is too small[42]. Therefore, the unpaired electrons in 3d channels are predominantly responsible for interacting with spin-polarized molecules. For O_2 molecule, which is triplet in its ground state (S = 3), when interacting with the CrPc (S = 5) and FePc (S = 3) sheets, the adsorption process leads the corresponding adducts to a lower spin state for both 2D CrPc-O_2 (S = 3) and 2D FePc-O_2 (S = 1), respectively. Only by donating spin up electrons in the 3d channels of Cr and Fe atoms to the unoccupied spin down LUMOs (2π*) in O_2 can such a lower spin state be achieved. For a CrPc sheet, the HOMO to HOMO-2 levels at the Γ point are all in the α (spin up) state. The doubly degenerate HOMO levels predominantly have a d_π character, whereas the HOMO-1 and HOMO-2 levels are mainly consisted of d_{z2} and d_{xy} components, respectively. All of the four levels lie in a notably higher energy range than their counterparts in a 2D FePc sheet. The spin up levels in 2D FePc are HOMO-2, HOMO-3, HOMO-4 and HOMO-6, as illustrated in Figure 3. In particular, the HOMO-3 orbital of a 2D CrPc sheet has a maximized overlap with the LUMO (2π*) of O_2 when the O_2 molecule adopts a parallel (side-on) adsorption configuration due to the symmetry reasons; while in a 2D FePc sheet, the dominating interacting orbitals with the unoccupied O_2 2π* orbitals are HOMO-2 and HOMO-3 exhibiting a d_π character, owing to their small energy difference with the LUMO of O_2. The adsorbed O_2 molecule will thus adopt an end-on configuration with a bent structure where the Fe-O-O angle is maximized for better orbital mixing. As a result of sufficient orbital overlapping, more charges will be transferred from the CrPc sheet to the adsorbed O_2 with respect to the case in 2D FePc (Table 1), giving rise to an elongated O-O bond length of 1.396 Å in a 2D CrPc sheet as compared with the value of 1.276 Å in a 2D FePc sheet.

However, the situation completely changes for CO adsorption. The central TM atoms interact with the adsorbed CO molecules via a well-established electron accepting and electron back-donating mechanism to form σ-π coordinate covalent bonds. The σ-π coordinate bond concerns essentially with the donation of CO lone pair (5σ orbital) to the empty d_{z2} orbital as well as the back-donation from the electron sufficient d_π orbital to the electron deficient 2π* orbital of CO. Therefore, the energy differences between these pertinent orbitals determine the interaction strength between the CO molecule and the TM central atom. In the case of a CrPc sheet, the electron-rich d_π orbitals are the doubly degenerate HOMOs lying higher in energy, which are facile to donate their electrons to the empty CO 2π* antibonding orbital. However, the electron-deficient d_{z2} orbital is LUMO + 9, and its energy is too high to achieve adequate hybridization with CO 5σ orbital. As a result, the unilateral electron donation from Cr to CO results in a negatively-charged adsorbed CO, as illustrated in Table 1. On the other hand, the electron-rich d_π orbitals of a FePc sheet not only contain the spin-up orbitals of HOMO-2 and HOMO-3, but also the HOMOs with spin-down. Additionally, contrary to the high-lying d_{z2} orbital of a CrPc sheet, the electron-deficient d_{z2} orbital of the FePc sheet is LUMO + 1 with a substantially lower energy, thereby enabling CO to inject more electrons to it. The bilateral electron injection between CO and Fe is responsible for the positively charging of the CO molecule adsorbed on a FePc sheet, as listed in Table 1. In summary, the pronounced distinctions between the CrPc and FePc sheets in the hybridizations between particular d orbitals and the frontier orbitals of CO and O_2 give rise to the opposite adsorption trends for CO and

Table 1 | Hirshfeld charges of CO and O_2 on 2D CrPc, MnPc and FePc sheets

	CrPc	MnPc	FePc
CO	−0.0396	−0.0007	0.0398
O_2	−0.3094	−0.1662	−0.0913

O_2. In the case of CO and O_2 adsorption on a MnPc sheet, the orbital arrangement of a 2D MnPc sheet is intermediate between the CrPc and FePc sheets. Therefore, the adsorption energies of CO and O_2 also lie between those on 2D CrPc and 2D FePc sheets. Based on the above analysis, we select a CrPc sheet for CO oxidation as discussed in the following.

Catalytic mechanism. Surface catalytic reactions proceed via a number of elementary adsorption/desorption steps whose reaction energetics are associated with the catalytic activity. On the basis of the Brønsted-Evans-Polanyi (BEP) relation, the activation energy barrier of an elementary reaction step ΔE can be interpreted as a linear function of the dissociative adsorption energy E_{ad} of each adsorbate involved in the step, providing us a preliminary empirical evaluation of the reaction facility[43,44]. Because of the notable E_{ad} of O_2 and CO on 2D Pc sheets in conjunction with the superb resistance to the CO poisoning effect, we only presented the energy barrier ΔE of the elementary reactions constituting the whole CO oxidation cycle on a 2D CrPc sheet in the following part, in order to determine the corresponding minimum energy pathway (MEP). We note that generally there are two well-established reaction mechanisms for the initiation steps involved in surface-catalyzed CO oxidation, namely the Langmuir-Hinshelwood (LH) mechanism and the Eley-Rideal (ER) mechanism[45]. In the former mechanism, the surface co-adsorbed and activated CO and O_2 molecules interact with each other via a concerted reaction pathway to form a peroxo-type like intermediate; while in the latter one, the free-standing CO directly reacts with a surface activated O_2 or atomic O generated through a surface motivated O_2 dissociation. Because the O_2 is strongly adsorbed and the O-O bond length is considerably elongated upon its adsorption on a 2D CrPc sheet, it seems that the ER mechanism would be more favorable. However, contrary to our expectation, after full TS search and geometry optimization, we find that no CO_2 is formed or other intermediate formation process exists, indicating that for this system the CO oxidation is *not* via the ER mechanism. Therefore, the LH mechanism $CO + O_2 \rightarrow OOCO \rightarrow CO_2 + O$ followed by the ER mechanism $CO + O \rightarrow CO_2$ is considered.

Figure 4 and Figure 5 show the energy profiles of MEPs via LH and ER mechanisms as well as the side and top views of the local configurations of the adsorbates along the MEPs, respectively. Upon coadsorption of CO and O_2, the CO and O_2 molecules approach each other to form the first transition state (TS1), with an energy barrier of 0.55 eV along the reaction pathway. Passing over TS1, an peroxide-type intermediate state (MS) is formed, which is a slight endothermic process with the reaction energy of 0.05 eV for $CO + O_2 \rightarrow OOCO$. Mediated by the central Cr atom, the O-O bond length of the peroxide-type intermediate elongates continuously and passes over the second transition state (TS2) with a substantially low energy barrier of only 0.09 eV to come to the final state (FS), releasing a large energy of 4.52 eV in the overall LH process. The resulting CO_2 molecule is easy to desorb from the substrate due to the weaker interaction between CO_2 and the substrate, leaving an atomic O strongly interacting with the Cr atom. Such an activated surface O atom can readily bind another CO molecule to form another intermediate state, surmounting an energy barrier of 0.46 eV. The intermediate state will soon turn to the final state without any energy barrier, regenerating a 2D CrPc sheet with another CO_2 released. The highest energy barrier of this catalytic cycle is therefore only 0.55 eV, which is considerably lower than that of Fe-N4 porphyrin-like graphene and carbon nanotube at the same calculation level of theory[16]. Such disparate energy barriers between Cr and Fe containing porphyrin-like frameworks further corroborate the fact that apposite selection of central metal atoms can achieve an outstanding performance in catalytic processes.

Temperature effect. Next we take the temperature effect into account to assess the reaction thermodynamics of the induced CO oxidation on a 2D CrPc sheet. It is well known that free energy change is determined by $\Delta G = \Delta H - T\Delta S$, where ΔG denotes the Gibbs free energy change in each step throughout the LH and ER mechanism, ΔH is the change in enthalpy, and ΔS is the change in entropy. ΔH contains two parts, namely ΔU and ΔPV. In our calculation, ΔU is defined as $\Delta U = \Delta E_{tot} + \Delta E_{vib} + \Delta E_{rot} + \Delta E_{trans}$, and ΔS is defined as $\Delta S = \Delta S_{vib} + \Delta S_{rot} + \Delta S_{trans}$. ΔE_{tot} is the standard DFT calculated electronic energy at 0 K, and the subscript vib, rot and trans are for the contribution of vibration, rotation and translation mode, respectively.

To get further insight into the temperature effect on ΔH and ΔS, we employ the following equations

$$\left(\frac{\partial(\Delta H)}{\partial T}\right)_p = \Delta C_p \qquad (1)$$

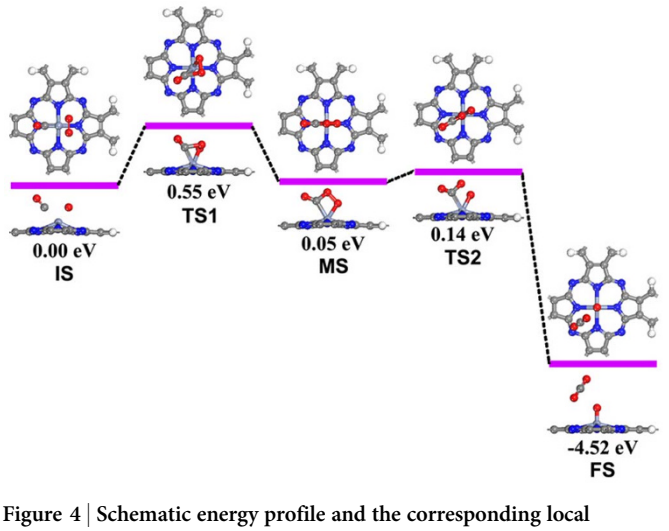

Figure 4 | Schematic energy profile and the corresponding local configurations along the Langmuir-Hinshelwood step. Both top (upper panel) and side views (lower panel) are illustrated. All energies are given with respect to the reference energy of the coadsorbed state for CO and O_2 on a 2D CrPc sheet.

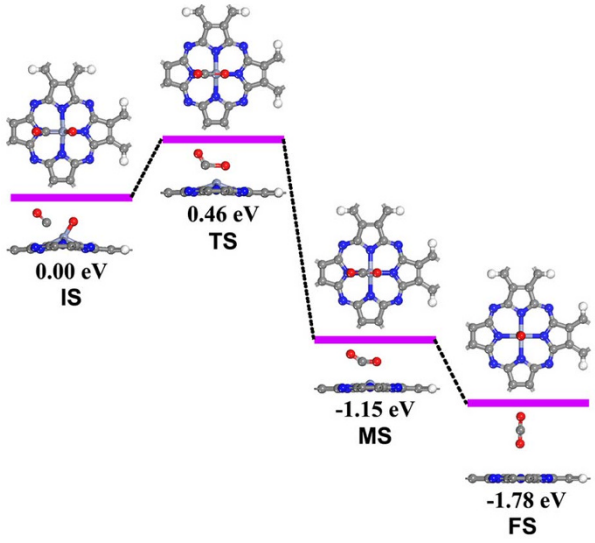

Figure 5 | Schematic energy profile and the corresponding local configurations along the Eley-Rideal step. Both top (upper panel) and side views (lower panel) are illustrated. All energies are given with respect to the reference energy of the coadsorbed state for CO and O on a 2D CrPc sheet.

Table 2 | Free energy changes (in eV) for each step in the catalytic CO oxidation reaction cycle under different temperatures

	LH Step			ER Step	
Temperature	IS-TS1(E_{a1})	MS-TS2(E_{a2})	IS-FS(E_{r1})	IS-TS(E_{a3})	IS-FS(E_{r2})
275 K	0.56	0.12	−4.56	0.46	−1.89
298.15 K	0.56	0.12	−4.56	0.46	−1.9
300 K	0.56	0.12	−4.56	0.46	−1.9
325 K	0.57	0.13	−4.56	0.46	−1.91
350 K	0.57	0.13	−4.56	0.46	−1.92
375 K	0.57	0.13	−4.56	0.46	−1.93
400 K	0.58	0.14	−4.57	0.46	−1.94
425 K	0.58	0.14	−4.57	0.47	−1.95
450 K	0.58	0.15	−4.57	0.47	−1.96
475 K	0.59	0.15	−4.57	0.47	−1.97

$$\Delta S(T_2) = \Delta S(T_1) + \int_{T_1}^{T_2} \frac{\sum_{\mathrm{B}} \nu_{\mathrm{B}} C_p(\mathrm{B}) dT}{T_2} \qquad (2)$$

where ΔC_p denotes the change of heat capacity at constant pressure and ν_B denotes stoichiometric number. The corrected free energy changes for the whole CO oxidation on a 2D CrPc sheet under different temperatures (275 K ~ 475 K) are listed in Table 2. We can see that although elevating the temperature can make the whole reaction thermodynamically more viable, the increased energy barriers for surmounting the three transition states hinders the dynamical feasibility. The activation energy barriers alter only slightly in the temperature range between 275 ~ 475 K, suggesting the notable stability and catalytic feasibility at lower temperatures as well as higher temperatures.

Electronic structure analysis. To unveil the microscopic scenario behind the peculiar catalytic activity of the 2D CrPc sheet, we calculated the local density of states projected onto the O1-O2 and the C-O bonds as well as the d-projected LDOS of Cr in IS, TS1, MS and TS2 of the LH step, respectively. As illustrated in Figure 6, the 2π* level of O_2 is partially shifted downward upon the adsorption in the IS state due to the notable charge transfer from the Cr atom. In

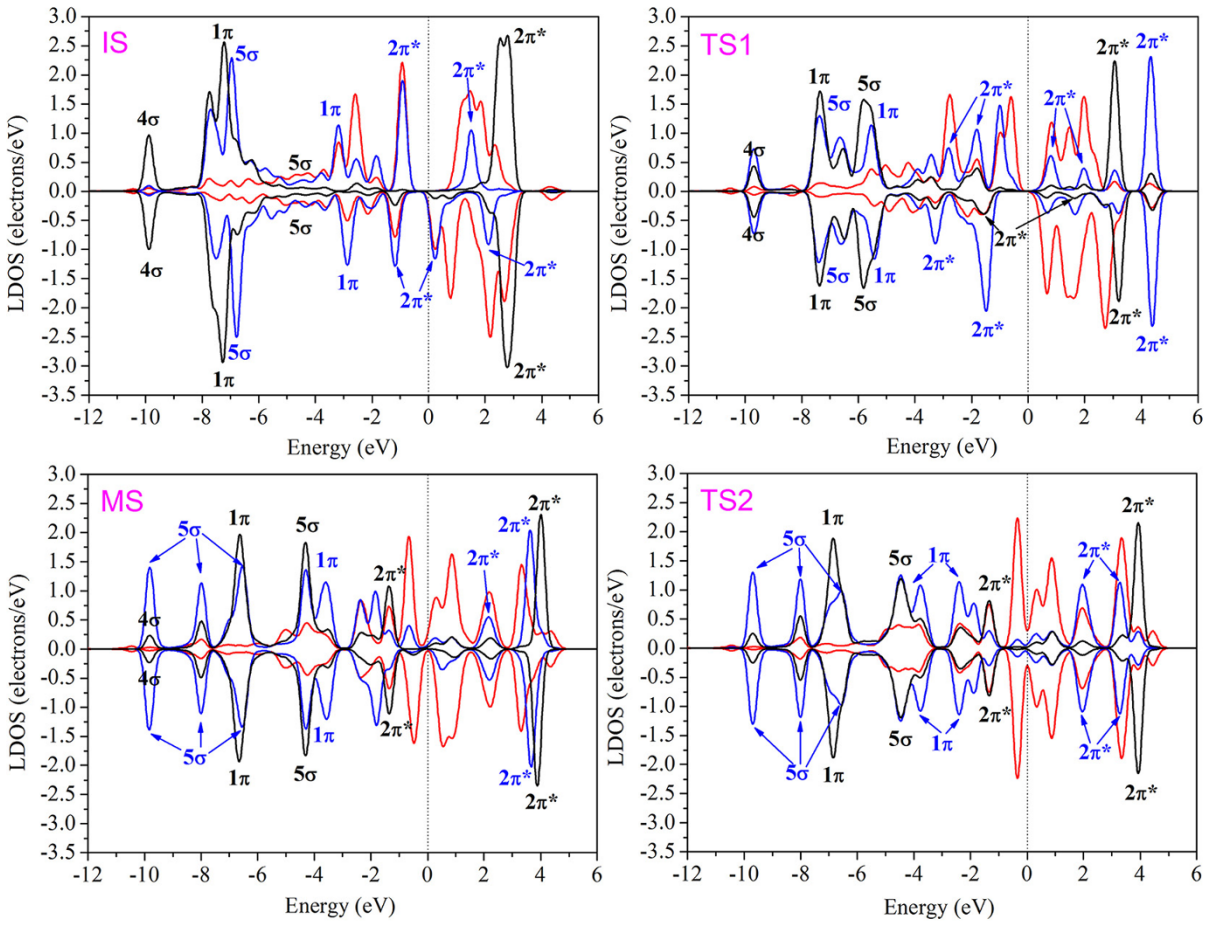

Figure 6 | Spin-polarized local density of states (LDOS) projected onto C-O and O1-O2 on a 2D CrPc sheet, as well as the d-projected LDOS of Cr in the IS, TS1, MS and TS2 in the LH step. Black solid curve for the LDOS projected on C-O; blue solid curve for the LDOS projected on O1-O2; red solid curve for the d-projected LDOS of the Cr atom. The corresponding orbital notations are also assigned.

contrast, the 2π* level of CO is still empty because of the paltry amount of charge transfer between CO and Cr. For the O1-O2 species on the 2D CrPc sheet, from IS to TS1, owing to the electronic resonance with CO 2π* state, the 2π* level of O_2 is further populated and broadened to hybridize with Cr 3d state to a larger extent. Meanwhile, the 2π* level of CO is also partially populated in the TS1 state. The O1-O2 1π state is elevated and becomes more involved with the Cr 3d state from TS1 to MS to TS2, which is ancillary in weakening the O1-O2 bond. The 2π* level of O1-O2 is gradually elevated upward as a result of the generation of the new C-O2 bond from TS1 to TS2. For the C-O species on the 2D CrPc, because of the end-on adsorption configuration, the 5σ level is shifted upward and strongly hybridized with the Cr 3d level in the whole LH step rather than the 1π level, which is one of the predominant factor in the dissociation of the O1-O2 bond because of the side-on adsorption configuration of O_2 molecule. Furthermore, the magnetism of the entire system is quenched at the TS2 state originating from the formation of the nonmagnetic CO_2 molecule and O adsorbed 2D CrPc sheet. Overall, mediated by the Cr 3d state, the O1-O2 1π and 2π* level interact strongly with the C-O 5σ and 2π* level. These electronic state resonances lead to the formation of C-O2 bond and the dissociation of O1-O2 bond, accelerating the catalytic elimination of the hazardous CO molecules.

Discussion

Based on first-principles calculations, we find that the 2D CrPc sheet exhibits superior catalytic activity towards CO oxidation withstanding CO poisoning effect. The exceptional catalytic activity can be ascribed to its peculiar orbital order, which enables the 2D CrPc sheet to interact strongly with O_2 while adsorbing CO only to a modest extent. The spin-up occupied d_π, d_{xy} and d_{z2} orbitals are majorly accountable to the electron injection to the O_2 void 2π* orbital. On the other hand, only three occupied d_π orbitals provide electrons to partially fill the empty CO 2π* orbital, the unoccupied d_{z2} orbital lies in a too high energy range to interact effectively with the CO 5σ orbital. Furthermore, we identified that the CO oxidation reaction catalyzed by the CrPc sheet proceeds first via Langmuir-Hinshelwood (LH) mechanism and then via Eley-Rideal (ER) mechanism with highest energy barrier of 0.55 eV, much lower than its Fe-containing counterparts, suggesting this reaction is viable to proceed at low temperature. Moreover, our vibrational analyses reveal that the 2D CrPc framework is viable in catalyzing the whole CO oxidation reaction at a wide temperature range without being significantly affected by temperature variation. The high activity of the 2D CrPc sheet along the LH step may be attributed to the electronic resonance among electronic states of CO, O_2, and the Cr atoms, particularly among the Cr-3d, CO-5σ, CO-2π*, and O2-2π* orbitals.

For avoiding the CO poisoning effect, PtAu alloy bimetallic catalysts and Pt overlayer-metal carbide catalysts have been suggested to improve the catalytic efficiency and lower the adsorption energy of CO to a moderate extent[46,47]. However, the low surface to volume ratio impedes further improvement to their catalytic activity. Although atoms or clusters loaded on pristine or defective carbon based material such as graphene showed high surface to volume ratios, previous calculations suggested that almost all of them suffer from different extent of CO poisoning effect. Due to the following advantages, the studied 2D CrPc sheet is superior to platinum based catalysts and carbon based nanocomposite catalysts: (1). The synthetic procedure of 2D TMPc sheets includes polymerization of small TCNB molecules and TM atoms, which creates no byproducts and is easily transferable to both metallic and insulating substrates, which is highly desirable in realistic device fabrication; (2). It possesses catalytically active unsaturated metal ions with lower valence states, and it exhibits comparable amount of available active metal sites with that in metal nanoparticles. To compare the catalytic efficiency of the 2D CrPc sheet with nanoparticles, we use the available catalytically active metal site number per gram instead of surface to volume ratio. In 2D CrPc, each structural unit contains 20 carbon atoms, 8 nitrogen atoms, 4 hydrogen atoms and 1 chromium atom. Therefore, The number of active metal sites in 1 gram of 2D CrPc sheet is $N_1 = \frac{1}{408} N_A = \frac{1}{408} \times 6.02 \times 10^{23} = 1.48 \times 10^{21}$. Which is comparable to the numbers of 1.87×10^{21} and 1.78×10^{21} for cuboctahedral Pt_{201} and icosahedral Au_{55} nanoparticles, respectively. (3). Cr atoms are uniformly distributed in 2D CrPc sheet without the problem of clustering which is often encountered in other substrates loaded with catalysts; (4). Different from the broad d band features of platinum based catalysts with nanocrystal structure, the d band of the sparsely distributed Cr atoms is sharp near the Fermi level and can be effectively tuned by other ways such as strains or chemical modification. These features discussed above make the 2D porous CrPc sheet very unique and promising in catalytic CO oxidation for large scale applications in industry.

Methods

Periodic spin-unrestricted density functional theory calculations were performed using the DMol^3 code[48,49]. The generalized gradient approximation (GGA) with the Perdew − Burke − Ernzerhof (PBE) functional was employed to describe the exchange and correlation potential[50]. DFT semicore pseudopotentials (DSPPs)[51] were used, where all-electron calculations were performed for C, O and N atoms, while the core electrons were replaced by a single effective pseudopotential including the relativistic effects for TM atoms. Double numerical plus polarization (DNP) basis set[48] was employed and the real space global orbital cutoff radius was set as 4.8 Å to ensure high quality results. We used a PBE-D scheme with the Grimme vdW correction[52,53], which has been well validated to describe the adsorption of small molecules on 2D nanomaterials[54].

We applied periodic boundary conditions with a vacuum space of 15 Å to avoid interactions between the TMPc sheet and its adjacent periodic images. A single unit cell was used to model the 2D TMPc systems because of the negligible effects of magnetic coupling between the unit cells on their catalytic properties. For geometry optimization and the search for the transition state (TS), the Brillouin zone was sampled with $5 \times 5 \times 1$ k points. For the electronic structure calculations, a Monkhorst-Pack scheme with $19 \times 19 \times 1$ k points grid meshes was employed. The atoms were fully relaxed without any symmetry constraints, with the convergence in energy, force and displacement being set at 1×10^{-5} Ha, 0.002 Ha/Å and 0.005 Å, respectively. All the self-consistent field (SCF) calculations were performed with the convergence criterion of 1×10^{-6} Ha without any smearing. The transition states were located through a complete LST/QST protocol involving linear synchronous transit (LST) maximization followed by repeated conjugated gradient (CG) refinements, and then several quadratic synchronous transit (QST) maximizations with repeated conjugated gradient (CG) refinements between them[55]. TS optimizations were carried out to confirm that the located TSs contain only one imaginary frequency. The nudged elastic band (NEB) method[56,57] was used to verify the MEP for elementary reaction steps.

1. Kummer, J. T. Catalysts for automobile emission control. *Prog. Energy Combust. Sci.* **6**, 177–199 (1980).
2. Greeley, J. & Mavrikakis, M. A First-Principles Study of Methanol Decomposition on Pt(111). *J. Am. Chem. Soc.* **124**, 7193–7201 (2002).
3. Langmuir, I. The mechanism of the catalytic action of platinum in the reactions $2CO + O_2 = 2CO_2$ and $2H_2 + O_2 = 2H_2O$. *Trans. Faraday Soc.* **17**, 621–654 (1922).
4. Heiz, U., Sanchez, A., Abbet, S. & Schneider, W. D. Catalytic Oxidation of Carbon Monoxide on Monodispersed Platinum Clusters: Each Atom Counts. *J. Am. Chem. Soc.* **121**, 3214–3217 (1999).
5. Allian, A. D. *et al.* Chemisorption of CO and Mechanism of CO Oxidation on Supported Platinum Nanoclusters. *J. Am. Chem. Soc.* **133**, 4498–4517 (2011).
6. Bunluesin, T., Cordatos, H. & Gorte, R. J. Study of CO Oxidation Kinetics on Rh/Ceria. *J. Catal.* **157**, 222–226 (1995).
7. Chen, M. S. *et al.* Highly active surfaces for CO oxidation on Rh, Pd, and Pt. *Surf. Sci.* **601**, 5326–5331 (2007).
8. Sanchez, A. *et al.* When Gold Is Not Noble: Nanoscale Gold Catalysts. *J. Phys. Chem. A* **103**, 9573–9578 (1999).
9. Lopez, N. & Nørskov, J. K. Catalytic CO Oxidation by a Gold Nanoparticle: A Density Functional Study. *J. Am. Chem. Soc.* **124**, 11262–11263 (2002).
10. Lopez, N. *et al.* On the origin of the catalytic activity of gold nanoparticles for low-temperature CO oxidation. *J. Catal.* **223**, 232–235 (2004).
11. Krasheninnikov, A. V., Lehtinen, P. O., Foster, A. S., Pyykkö, P. & Nieminen, R. M. Embedding Transition-Metal Atoms in Graphene: Structure, Bonding, and Magnetism. *Phys. Rev. Lett.* **102**, 126807 (2009).

12. Lu, Y.-H., Zhou, M., Zhang, C. & Feng, Y.-P. Metal-Embedded Graphene: A Possible Catalyst with High Activity. *J. Phys. Chem. C* **113**, 20156–20160 (2009).
13. Li, Y., Zhou, Z., Yu, G., Chen, W. & Chen, Z. CO Catalytic Oxidation on Iron-Embedded Graphene: Computational Quest for Low-Cost Nanocatalysts. *J. Phys. Chem. C* **114**, 6250–6254 (2010).
14. Song, E. H., Wen, Z. & Jiang, Q. CO Catalytic Oxidation on Copper-Embedded Graphene. *J. Phys. Chem. C* **115**, 3678–3683 (2011).
15. Wannakao, S., Nongnual, T., Khongpracha, P., Maihom, T. & Limtrakul, J. Reaction Mechanisms for CO Catalytic Oxidation by N_2O on Fe-Embedded Graphene. *J. Phys. Chem. C* **116**, 16992–16998 (2012).
16. Zhang, P., Chen, X. F., Lian, J. S. & Jiang, Q. Structural Selectivity of CO Oxidation on Fe/N/C Catalysts. *J. Phys. Chem. C* **116**, 17572–17579 (2012).
17. Banhart, F., Kotakoski, J. & Krasheninnikov, A. V. Structural Defects in Graphene. *ACS Nano* **5**, 26–41 (2010).
18. Abel, M., Clair, S., Ourdjini, O., Mossoyan, M. & Porte, L. Single Layer of Polymeric Fe-Phthalocyanine: An Organometallic Sheet on Metal and Thin Insulating Film. *J. Am. Chem. Soc.* **133**, 1203–1205 (2010).
19. Jasinski, R. A New Fuel Cell Cathode Catalyst. *Nature* **201**, 1212–1213 (1964).
20. Tanaka, A. A., Fierro, C., Scherson, D. & Yaeger, E. B. Electrocatalytic aspects of iron phthalocyanine and its. mu.-oxo derivatives dispersed on high surface area carbon. *J. Phys. Chem.* **91**, 3799–3807 (1987).
21. Arechederra, R. L., Artyushkova, K., Atanassov, P. & Minteer, S. D. Growth of Phthalocyanine Doped and Undoped Nanotubes Using Mild Synthesis Conditions for Development of Novel Oxygen Reduction Catalysts. *ACS Appl. Mater. Interfaces* **2**, 3295–3302 (2010).
22. Cao, R. *et al*. Promotion of oxygen reduction by a bio-inspired tethered iron phthalocyanine carbon nanotube-based catalyst. *Nat. Commun.* **4**, 2036(2013).
23. Kapusta, S. & Hackerman, N. Carbon Dioxide Reduction at a Metal Phthalocyanine Catalyzed Carbon Electrode. *J. Electrochem. Soc.* **131**, 1511–1514 (1984).
24. Abe, T. *et al*. Factors affecting selective electrocatalytic CO_2 reduction with cobalt phthalocyanine incorporated in a polyvinylpyridine membrane coated on a graphite electrode. *J. Electroanal. Chem.* **412**, 125–132 (1996).
25. He, H. *et al*. Molecular and Electronic Structures of Transition-Metal Macrocyclic Complexes as Related to Catalyzing Oxygen Reduction Reactions: A Density Functional Theory Study. *J. Phys. Chem.C* **116**, 16038–16046 (2012).
26. Nielsen, I. M. B. & Leung, K. Cobalt−Porphyrin Catalyzed Electrochemical Reduction of Carbon Dioxide in Water. 1. A Density Functional Study of Intermediates. *J. Phys. Chem. A* **114**, 10166–10173 (2010).
27. Leung, K., Nielsen, I. M. B., Sai, N., Medforth, C. & Shelnutt, J. A. Cobalt−Porphyrin Catalyzed Electrochemical Reduction of Carbon Dioxide in Water. 2. Mechanism from First Principles. *J. Phys. Chem. A* **114**, 10174–10184 (2010).
28. Weber, C. *et al*. Importance of Many-Body Effects in the Kernel of Hemoglobin for Ligand Binding. *Phys. Rev. Lett.* **110**, 106402 (2013).
29. Nguyen, T. Q., Escaño, M. C. S. & Kasai, H. Nitric Oxide Adsorption Effects on Metal Phthalocyanines. *J. Phys. Chem. B* **114**, 10017–10021 (2010).
30. Zhou, J. & Sun, Q. Magnetism of Phthalocyanine-Based Organometallic Single Porous Sheet. *J. Am. Chem. Soc.* **133**, 15113–15119 (2011).
31. Zhou, J., Wang, Q., Sun, Q., Kawazoe, Y. & Jena, P. Strain-Induced Spin Crossover in Phthalocyanine-Based Organometallic Sheets. *J. Phys. Chem. Lett.* **3**, 3109–3114 (2012).
32. Zhou, J. & Sun, Q. Absorption induced modulation of magnetism in two-dimensional metal-phthalocyanine porous sheets. *J. Chem. Phys.* **138**, 204706 (2013).
33. Zhou, J. & Sun, Q. Carrier induced magnetic coupling transitions in phthalocyanine based organometallic sheet. *Nanoscale* **6**, 328–333 (2014).
34. Lü, K. *et al*. Sc-phthalocyanine sheet: Promising material for hydrogen storage. *Appl. Phys. Lett.* **99**, 163104 (2011).
35. Lü, K. *et al*. Pre-combustion CO_2 capture by transition metal ions embedded in phthalocyanine sheets. *J. Chem. Phys.* **136**, 234703 (2012).
36. Remediakis, I. N., Lopez, N. & Nørskov, J. K. CO Oxidation on Rutile-Supported Au Nanoparticles. *Angew. Chem. Int. Ed.* **44**, 1824–1826 (2005).
37. Harding, C. *et al*. Control and Manipulation of Gold Nanocatalysis: Effects of Metal Oxide Support Thickness and Composition. *J. Am. Chem. Soc.* **131**, 538–548 (2008).
38. Tang, D. & Hu, C. DFT Insight into CO Oxidation Catalyzed by Gold Nanoclusters: Charge Effect and Multi-State Reactivity. *J. Phys. Chem. Lett.* **2**, 2972–2977 (2011).
39. Reber, A. C., Khanna, S. N., Roach, P. J., Woodward, W. H. & Castleman, A. W. Spin Accommodation and Reactivity of Aluminum Based Clusters with O_2. *J. Am. Chem. Soc.* **129**, 16098–16101 (2007).
40. Burgert, R. *et al*. Spin Conservation Accounts for Aluminum Cluster Anion Reactivity Pattern with O_2. *Science* **319**, 438–442 (2008).
41. Wigner, E. & Witmer, E. E. About the Structure of the diatomic Mulecule Spectra according to Quantum Mechanics. *Z. Phys.* **51**, 859–886 (1928).
42. Orellana, W. Catalytic Properties of Transition Metal–N4 Moieties in Graphene for the Oxygen Reduction Reaction: Evidence of Spin-Dependent Mechanisms. *J. Phys. Chem. C* **117**, 9812–9818 (2013).
43. Bligaard, T. *et al*. The Brønsted–Evans–Polanyi relation and the volcano curve in heterogeneous catalysis. *J. Catal.* **224**, 206–217 (2004).
44. Kim, G., Kawazoe, Y. & Lee, K.-R. Controlled Catalytic Properties of Platinum Clusters on Strained Graphene. *J. Phys. Chem. Lett.* **3**, 1989–1996 (2012).
45. An, W., Pei, Y. & Zeng, X. C. CO Oxidation Catalyzed by Single-Walled Helical Gold Nanotube. *Nano Lett.* **8**, 195–202 (2007).
46. Gao, F. & Goodman, D. W. Pd-Au bimetallic catalysts: understanding alloy effects from planar models and (supported) nanoparticles. *Chem. Soc. Rev.* **41**, 8009–8020 (2012).
47. Kelly, T. G. & Chen, J. G. Metal overlayer on metal carbide substrate: unique bimetallic properties for catalysis and electrocatalysis. *Chem. Soc. Rev.* **41**, 8021–8034 (2012).
48. Delley, B. An all-electron numerical method for solving the local density functional for polyatomic molecules. *J. Chem. Phys.* **92**, 508–517 (1990).
49. Delley, B. From molecules to solids with the $DMol^3$ approach. *J. Chem. Phys.* **113**, 7756–7764 (2000).
50. Perdew, J. P., Burke, K. & Ernzerhof, M. Generalized Gradient Approximation Made Simple. *Phys. Rev. Lett.* **77**, 3865–3868 (1996).
51. Delley, B. Hardness conserving semilocal pseudopotentials. *Phys. Rev. B* **66**, 155125 (2002).
52. Grimme, S. Accurate description of van der Waals complexes by density functional theory including empirical corrections. *J.Comput. Chem.* **25**, 1463–1473 (2004).
53. Grimme, S. Semiempirical GGA-type density functional constructed with a long-range dispersion correction. *J. Comput. Chem.* **27**, 1787–1799 (2006).
54. Jiang, Q. G., Ao, Z. M., Chu, D. W. & Jiang, Q. Reversible Transition of Graphene from Hydrophobic to Hydrophilic in the Presence of an Electric Field. *J. Phys. Chem. C* **116**, 19321–19326 (2012).
55. Halgren, T. A. & Lipscomb, W. N. The synchronous-transit method for determining reaction pathways and locating molecular transition states. *Chem. Phys. Lett.* **49**, 225–232 (1977).
56. Mills, G. & Jónsson, H. Quantum and thermal effects in H_2 dissociative adsorption: Evaluation of free energy barriers in multidimensional quantum systems. *Phys. Rev. Lett.* **72**, 1124–1127 (1994).
57. Henkelman, G. & Jonsson, H. Improved tangent estimate in the nudged elastic band method for finding minimum energy paths and saddle points. *J. Chem. Phys.* **113**, 9978–9985 (2000).

Acknowledgments

This work is partially supported by grants from the National Natural Science Foundation of China (NSFC-21173007 and 11274023), and from the National Grand Fundamental Research 973 Program of China (2012CB921404).

Author contributions

Q.S. designed research; Y.L. performed research.

Additional information

Competing financial interests: The authors declare no competing financial interests.

How to cite this article: Li, Y.W. & Sun, Q. The superior catalytic CO oxidation capacity of a Cr-phthalocyanine porous sheet. *Sci. Rep.* **4**, 4098; DOI:10.1038/srep04098 (2014).